Drivers of chorus in the outer dayside magnetosphere

M. Spasojevic[1] and U. S. Inan[1,2]

Received 12 May 2009; revised 15 October 2009; accepted 16 November 2009; published 29 April 2010.

[1] Using ELF/VLF wave data recorded in 2007 from two high-latitude (Λ = 69.8°, 71.8°) Antarctic ground stations, the dayside variation of chorus wave occurrence and amplitude are analyzed in conjunction with geomagnetic and solar wind driving parameters. Both stations observe chorus (defined here as discrete rising emission tones together with unstructured hiss) in a broad window of local time across the dayside when the stations are on closed magnetic field lines. Wave occurrence rates rise rapidly from ~0.06–0.12 at dawn to their maximum value of ~0.5–0.6 near local noon. The event amplitudes also peak near noon. Occurrence probabilities at the lower-latitude station are consistently higher with the average difference in the rate between the two stations being 0.15. In addition, ~80% of the time, event amplitudes are larger at the lower-latitude site. When the stations are in the dawn local time sector (5.5 < MLT < 10), the onset of waves is clearly linked to substorms, as seen by the *AE* index as well as by energetic electron injections observed at geosynchronous orbit. However, as the stations rotate to noon (MLT > 10), wave occurrence rates appear to be relatively independent of geomagnetic activity as measured by K_p and *AE*. Chorus near noon at times appears related to substorm activity, but intense waves can also be observed during extended quiet periods. Waves across the entire dayside are more likely during higher solar wind dynamic pressure as well as during significant changes in pressure. We attribute the high occurrence rate of outer dayside chorus to several effects resulting from solar wind compression of the dayside magnetosphere; the first is electron drift shell splitting, and the second is the creation of a region of high magnetic field homogeneity which is particularly favorable for wave growth.

Citation: Spasojevic, M., and U. S. Inan (2010), Drivers of chorus in the outer dayside magnetosphere, *J. Geophys. Res.*, *115*, A00F09, doi:10.1029/2009JA014452.

1. Introduction

[2] Chorus is an intense electromagnetic, whistler mode wave that is generated in the low-density region between the plasmapause and the magnetopause and can be observed on the ground over a range of latitudes [e.g., *Sazhin and Hayakawa*, 1992, and references therein]. Being a plasma wave mode of particular geophysical interest, chorus is believed to play a major role in the evolution of energetic electron distributions within the magnetosphere. Chorus is a driver of pulsating aurora and the morningside diffuse aurora [*Inan et al.*, 1992, and references therein], and resonant wave-particle interactions can also lead to much higher energy (>1 MeV) electron microburst precipitation [e.g., *Lorentzen et al.*, 2001; *O'Brien et al.*, 2004]. In addition to losses, these resonant interactions can result in the acceleration of ring current electrons up to relativistic energies [e.g., *Horne et al.*, 2005; *Summers et al.*, 2007].

[3] In order to assess the role of chorus in electron acceleration and loss, it is necessary to understand the global distribution of waves within the magnetosphere as well as the solar wind and magnetospheric drivers that favor wave growth. In this paper, we present a statistical study of the occurrence and driving parameters for dayside chorus as observed by a pair of high invariant latitude ground stations. These emissions are sometimes referred to as polar chorus as a result of their measurement on the ground in the Earth's polar regions [*Ungstrup and Jackerott*, 1963].

[4] Chorus is generated through the electron cyclotron instability by anisotropic ($T_\perp > T_\parallel$) distributions of energetic electrons in the range of 5 to 150 keV [*Tsurutani and Smith*, 1974; *Thorne et al.*, 1977]. These unstable distributions can result from substorm particle injections, and correspondingly, chorus is predominantly observed across the morning and noon local time sectors of the Earth in association with eastward drifting electrons [e.g., *Burtis and Helliwell*, 1976]. Chorus exhibits a magnetic local time variation that is dependent on *L* shell [e.g., *Pope*, 1960; *Tsurutani and Smith*, 1977]. In the region just outside the plasmapause, the maximum occurrence of chorus is in the postmidnight sector. This local time maximum increases with increasing

[1]Space, Telecommunications, and Radioscience Laboratory, Stanford University, Stanford, California, USA.
[2]Koc University, Istanbul, Turkey.

0148-0227/10/2009JA014452

L such that in the outer magnetosphere the daily occurrence maximum of chorus is centered near noon [*Pope*, 1960].

[5] In the middle magnetosphere ($L \simeq 4$ to 8) the onset of wave generation has been demonstrated to be well associated with substorms. In particular, *Tsurutani and Smith* [1974] first showed that the distribution of chorus as a function of L shell and MLT in the postmidnight sector was similar to that of enhanced substorm-injected electrons with energies >40 keV. Several studies have shown correlation between chorus occurrence and substorms as measured by the *AE* index [*Tsurutani and Smith*, 1977; *Thorne et al.*, 1977; *Meredith et al.*, 2001]. Using ground-based observations from Halley, Antarctica at $L = 4$, *Smith et al.* [1999] compared chorus observations with colocated magnetometer signals and showed that chorus onset was coincident with substorm onset. Strong correlation has also been observed between chorus observations at $L = 4$ and electron injections as observed by geostationary spacecraft [*Smith et al.*, 1999; *Abel et al.*, 2006]. In addition, *Abel et al.* [2006] found that 25% of substorm chorus events are associated with the electron drift echo which occurs on the order of 30 to 90 min after the initial injection as the source electrons drift completely around the Earth.

[6] At L shells of 4–8, Poynting flux measurements have shown chorus to be generated near the geomagnetic equator [*LeDocq et al.*, 1998; *Santolík et al.*, 2003; *Parrot et al.*, 2003; *Santolík et al.*, 2005a]. A number of studies have also shown that chorus is narrowly confined to the equatorial plane on the nightside (primarily observed within 5–10° of the magnetic equator), but on the dayside, waves are observed over a much wider range of latitudes (regularly extending at least 25° off the equator) [e.g., *Burton and Holzer*, 1974; *Tsurutani and Smith*, 1977; *Meredith et al.*, 2001; *Li et al.*, 2009].

[7] The general morphology of chorus observed in the outer dayside magnetosphere ($L \gtrsim 8$) is different from that at lower L values. Several additional studies have found that chorus in the outer dayside magnetosphere has a relatively high overall occurrence rate compared with other magnetospheric regions [*Tsurutani and Smith*, 1977; *Koons and Roeder*, 1990; *Santolík et al.*, 2005b; *Li et al.*, 2009]. *Tsurutani and Smith* [1977] reported chorus emissions on the dayside, at $8 \leq \mathrm{MLT} \leq 16$, within a few R_E of the magnetopause. These emissions tended to be observed off the equator at latitudes >15° and thus were dubbed by the authors as "high-latitude" chorus. *Tsurutani and Smith* [1977] found no statistical correlation between high-latitude chorus and substorms as measured by the *AE* index. Although some of the events did appear in the aftermath of substorms, many of the chorus observations occurred during periods of extreme geomagnetic quiet. Recently, *Li et al.* [2009] found that chorus in the dayside outer magnetosphere at latitudes in the range of ~0–25° also occurs over a wide range of *AE* activity including quiet intervals. Ground-based observations of chorus suggest that wave generation in the outer magnetosphere is related to the solar wind dynamic pressure. Compressions during sudden commencement geomagnetic storms have been shown to trigger chorus or increase its intensity [*Gail et al.*, 1990]. At times, the dynamic pressure appears to directly control wave generation with the wave amplitude tracking the pressure changes for many hours [*Salvati et al.*, 2000].

[8] *Tsurutani and Smith* [1977] speculated that outer dayside chorus is generated in so-called "minimum-B pockets." These are regions in the outer dayside magnetosphere near the magnetopause where the minimum magnetic field value moves from the equator to an off-equatorial location as a result of solar wind compression of the dayside magnetopause. There will typically exist a minimum-B pocket on either side of the equator although the exact size and shape of the regions depend on the dipole tilt and solar wind parameters [e.g., *Shabansky*, 1971]. Observational evidence supporting the idea of off-equatorial generation has been relatively sparse. *Vaivads et al.* [2007] reported a single case of chorus generation at an off-equatorial location corresponding to a local minimum of the magnetic field. *Tsurutani et al.* [2009] showed two high-latitude chorus events where the Poynting flux was directed toward the equator possibly indicating generation in the minimum-B pockets.

[9] Despite past work on outer dayside chorus, there are still unanswered questions concerning why this is a preferred source region for the waves, what allows them to persist during quiet intervals, and what is the role of the minimum-B pockets in wave generation. Here we present further statistics on outer dayside chorus gathered from ground-based observations, examine the solar wind and magnetospheric drivers of the waves, and discuss several factors that likely contribute to the high occurrence rates in the noon sector related to magnetic field configuration.

2. Diurnal Wave Pattern

[10] The Automatic Geophysical Observatories (AGO) form an array of unmanned geophysical observing stations across the Antarctic plateau. The two lowest geomagnetic latitude stations are P2 (geographic: 85.67° S, 313.62° E, geomagnetic: $\Lambda = -69.84°$, MLT = UT − 3.5 h) and P3 (geographic: 82.75° S, 28.59° E, geomagnetic: $\Lambda = -71.80°$, MLT = UT − 2.0 h). An ELF/VLF receiver system at each site records, continuously in multiple frequency-banded channels as well as in broadband snapshots, wave activity incident upon two orthogonal loop antennas. Figure 1a shows a typical example of the diurnal pattern of ELF/VLF wave activity recorded at P2 and P3 by the frequency-banded system. The system records, twice per second, the average amplitude in a set of band-pass filtered frequency channels from 0.5 to 40 kHz (decreasing in frequency from top to bottom in Figure 1a).

[11] When the stations are on the nightside ($2000 \lesssim \mathrm{UT} \lesssim 0800$) they lie on magnetic field lines that thread the auroral zone. In this region, auroral hiss is often observed, occurring primarily at frequencies above 2 kHz. In Figure 1a, two forms of auroral hiss can be seen [e.g., *Sazhin et al.*, 1993] with impulsive auroral hiss seen at both P2 and P3 around 2100 UT while continuous auroral hiss is observed at P2 from 0000 to 0900 UT. Although the receivers measure only up to 40 kHz, auroral hiss can extend to much higher frequencies at times exceeding 500 kHz [e.g., *LaBelle et al.*, 1998].

[12] When the stations rotate to the dayside ($0800 \lesssim \mathrm{UT} \lesssim 2000$), they typically lie on closed magnetic field lines that map to the outer magnetosphere. During this time, the stations tend to observe only low-frequency emissions, as

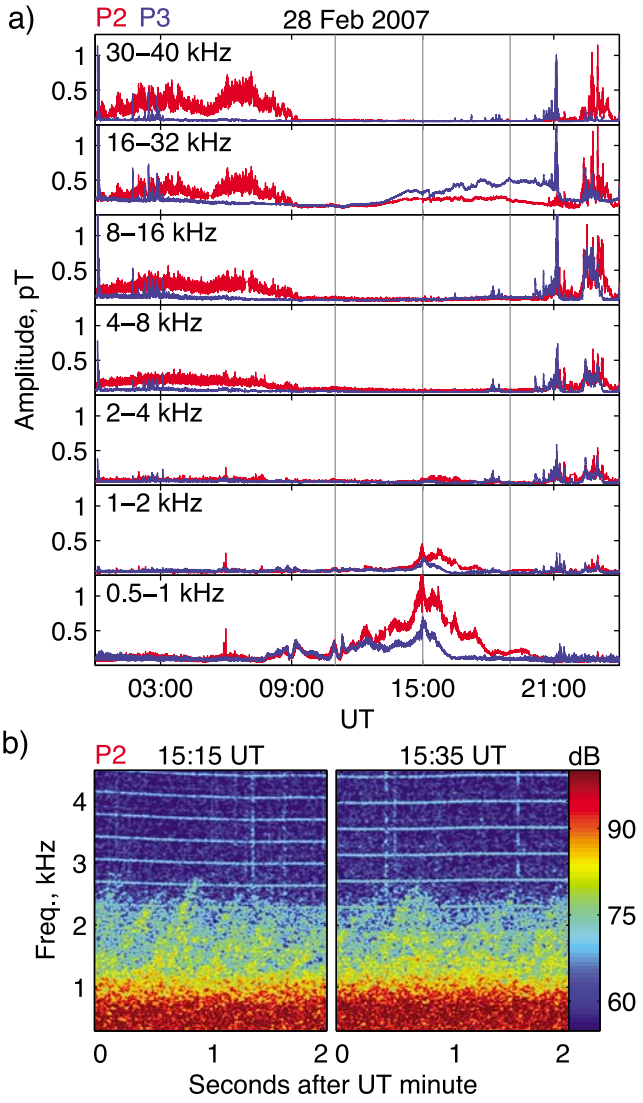

Figure 1. (a) A 24 h data record from the frequency-banded ELF/VLF receiver system from AGO stations P2 (red) and P3 (blue). The vertical lines indicate the times (1100, 1500, and 1900 UT) of the displayed ELF/VLF viewing area in Figure 2. (b) Two 2 s spectrograms from the broadband ELF/VLF snapshot receiver from P2.

seen in the bottom channels of Figure 1a. In addition to the continuous recordings of wave amplitude in the frequency-banded channels, the ELF/VLF system records full waveform data up to 4.5 kHz in brief snapshots (2 s every 5 min). The waveform data is used to identify the emission type via the spectral characteristics. Figure 1b shows two such snapshots from P2, with discrete rising elements, characteristic of chorus, clearly evident above ~1 kHz. At lower frequencies (below ~1 kHz), the emissions resemble a structureless hiss emission. The spectral characteristics in Figure 1b are typical for observations at the AGO sites on the dayside and are consistent with previous reports of polar chorus [e.g., *Ungstrup and Jackerott*, 1963].

[13] Chorus and hiss are closely associated emissions. In analysis of in situ observations including those close to the equatorial source region, *Cornilleau-Wehrlin et al.* [1978, p. 381] concluded that "chorus is almost always associated with hiss." Propagation effects can further convert discrete chorus emissions into a hiss-like spectrum. *Santolík et al.* [2006] showed that individual chorus wave packets can be dispersed and mixed together as a result of nonducted propagation from the source region to low altitudes resulting in the formation of so-called ELF hiss (a low-altitude emission found outside the plasmapause primarily on the dayside [e.g., *Gurnett and O'Brien*, 1964]). In addition, a ground-based receiver may observe waves coming from a distributed set of ionospheric exit points, which will tend to mix the structured chorus into a hiss-like spectrum. For the remainder of this paper, we will refer to the low-frequency emissions observed by the stations on the dayside simply as chorus while recognizing that they most often appear as discrete rising emissions together with unstructured hiss. We also note that overall the emissions tend to be more structured and chorus-like when they are more intense while the weaker emissions tend to be more hiss-like.

[14] As seen in Figure 1a, chorus at P2 and P3 is strongest in the lowest available frequency channel (0.5–1 kHz) although as its intensity increases so does the bandwidth of the waves, at times extending up to ~3 kHz. The wave pattern seen in Figure 1a is fairly characteristic with an onset of chorus in the dawn local time, peak intensity near local noon, and decreasing wave amplitude toward dusk. However, over the course of the day the wave amplitude can vary considerably; in Figure 1a, for example, local wave amplitude maxima can be seen every couple of hours.

[15] Figure 2 shows the location of the stations mapped along geomagnetic field lines to the GSM equatorial plane using the T01 magnetic field model [*Tsyganenko*, 2002a, 2002b] under nominal solar wind conditions for chorus observation (B_z = 2 nT, P_{sw} = 3 nPa). Although located only 2° equatorward of P3, station P2 maps to the equatorial plane at least 1 R_E (depending on the local time) earthward of P3.

[16] A single high-latitude ground station can observe ELF/VLF waves generated over a broad magnetospheric region. This occurs for a variety of reasons. First of all, once waves penetrate the ionosphere, they can propagate with relatively low attenuation for several hundred kilometers in the Earth-ionosphere waveguide [*Tsuruda et al.*, 1982]. In order to penetrate the ionosphere, the wave must have a nearly vertical incident angle at the topside of the ionosphere [*Helliwell*, 1965, section 3.7], which corresponds to a nearly field-aligned wave normal angle at these high geomagnetic latitudes. Field-aligned incidence onto the ionosphere can result from propagation in a field-aligned density irregularity or duct [*Smith et al.*, 1960]. Recent results from the Radio Plasma Imager on board the IMAGE spacecraft have shown that the magnetosphere is permeated by irregular density structures that support ducted wave propagation over a wide range of frequencies (see review by *Masson et al.* [2009]). Alternatively, ELF/VLF waves propagating in a nonducted mode, at frequencies below half of the equatorial gyrofrequency, can reach the ionosphere with vertical incidence through a set of specialized ray paths. *Chum and Santolík* [2005] showed that waves launched at the equator in a dipole field with wave normal angle near the Gendrin angle (θ_G = arccos $\frac{2\omega}{\omega_{ce}}$) and directed Earthward will reach the ionosphere with nearly vertical incidence. This

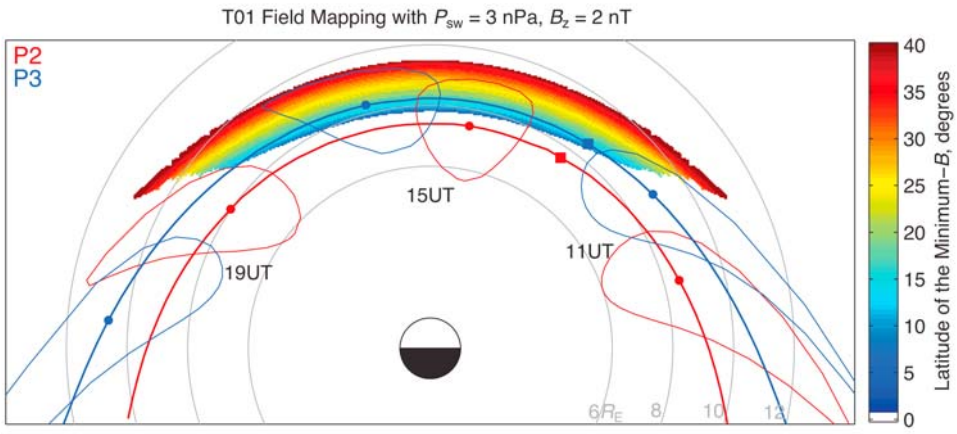

Figure 2. Location of the ground stations mapped along geomagnetic field to the GSM equatorial plane using the T01 magnetic field model with solar wind pressure P_{sw} = 3 nPa and IMF B_z = 2 nT for P2 (heavy red line) and P3 (heavy blue line). In addition, at selected UT times the estimated ELF/VLF viewing area (500 km circle in the ionosphere) is also mapped along field lines to the equator for P2 (thin red line) and P3 (thin blue line). The dots indicate the mapped location of the stations at 1100, 1500, and 1900 UT, while the square indicates the location at 10 MLT (in the ionosphere). The rainbow color scale indicates the latitude of the minimum magnetic field value along the field line that crosses the equator at that point.

nonducted propagation will result in significant inward cross-L propagation. Waves that reach the topside ionosphere with higher wave normal angles may, at times, also penetrate to the ground. *Sonwalkar and Harikumar* [2000] showed that meter-scale density irregularities in the topside ionosphere can scatter high wave normal angle waves to lower angles and into the ionospheric transmission cone.

[17] In addition to the mapped location of the stations, Figure 2 shows the estimated maximal extent of the ELF/VLF viewing area at three selected times (1100, 1500, and 1900 UT). The ELF/VLF viewing area was estimated by tracing field lines originating in the ionosphere in a 500 km circle around the station. The cross-L propagation effect discussed above may additionally extend the viewing area toward the magnetopause, but confirmation of the effect reported by *Chum and Santolík* [2005] in a realistic magnetic field is needed for the high geomagnetic latitudes of the AGO stations. In Figure 1a, chorus intensities reach a peak value near 1500 UT. At this time, the stations are in the noon local time sector, and we estimate that the waves originated on field lines that cross the GSM equatorial plane at radial distances of 6–9 R_E.

[18] Chorus observed on the ground is generally assumed to be lower band chorus (defined as having been generated in the range of 0.1–0.5 of the equatorial gyrofrequency) since upper band chorus (0.5–0.8 of the equatorial gyrofrequency) cannot be guided along the field line within field-aligned density enhancements. However, upper band waves can be efficiently guided along field-aligned density depletions or troughs [*Smith et al.*, 1960] and thus impinge on the ionosphere within the ionospheric transmission cone. Nevertheless, upper band chorus is typically 1 to 2 orders of magnitude weaker than lower band chorus as measured near the source region [e.g., *Meredith et al.*, 2001] and propagation through the ionosphere further attenuates the waves. In addition, upper band chorus is unlikely to penetrate the ionosphere after propagation in a nonducted mode, since waves in this frequency range quickly move toward the resonance cone as they propagate away from the source region [e.g., *Lauben et al.*, 2002]. For the above reasons, we expect that the vast majority of waves observed here are indeed lower band chorus emissions.

3. Wave Occurrence Probability and Amplitude

[19] The goal of the present study is to understand the amplitude variability of dayside chorus as observed at high invariant latitude in terms of solar wind and magnetospheric drivers. We examine chorus activity at AGO P2 and P3 for the first 103 days in 2007. It should be noted that this period was an interval of low solar activity during which the K_p index did not exceed 5^+. We divide the data set into 30 min intervals and define a chorus event as an interval over which the median wave amplitude is ≥0.16 pT in the 0.5–1 kHz band. In order to eliminate intervals of auroral hiss, an additional criteria is that the median wave amplitude in the 4–8 kHz channel must also remain below 0.16 pT for the same period. These criteria were developed based on visual examination of the frequency-banded and broadband data records for the 2007 data set. The chorus event amplitude is defined as the median wave amplitude in the 30 min interval. A median value is used since, at times, the data is spiky as a result of contamination from lightning-generated radio atmospherics.

[20] Figure 3a shows the chorus event occurrence probability at the two stations as a function of local time for the 103 day study period. The occurrence probability of chorus observed at P2 is ~0.5–0.6 in a broad window around local noon and falls off to <0.15 toward dawn and dusk. The occurrence probability at P3 follows a similar pattern, but the rates are lower by 0.15 on average. Also, the noon peak is narrower at P3, that is the occurrence rates fall off more

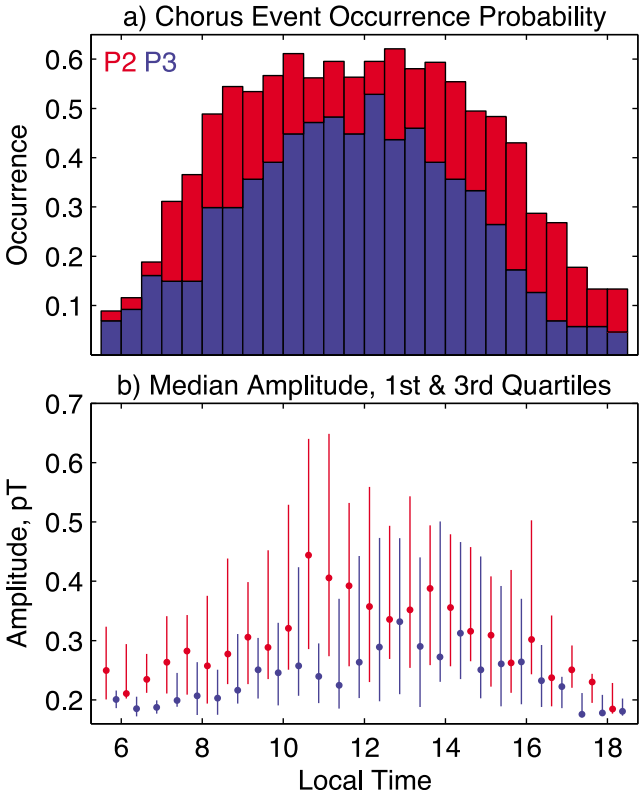

Figure 3. (a) The chorus event occurrence probability as a function of local time for P2 (red) and P3 (blue). (b) The median event amplitude (dot) and range of the first and third quartiles (vertical line) also as a function of local time for the two stations.

sharply toward dawn and dusk. Occurrence probabilities are most similar between the two stations close to local dawn where the difference in the occurrence rate is <0.03.

[21] Figure 3b shows the distribution of chorus event amplitudes with the dot indicating the median event amplitude and the line indicating the range of the first and third quartiles of the distribution. At P2, the event amplitude tends to increase from dawn to noon (with the largest amplitudes observed just prior to local noon) and then decrease in the post noon sector. Similar to the occurrence probability, the event amplitudes at P3 tend to be smaller than at P2. In addition, the event amplitudes at P3 tend to peak just post local noon, and at that time the range of the event amplitudes is the most similar between the two stations at 0.25–0.45 pT.

4. Wave Drivers: Case Events

[22] Next, we examine the occurrence of chorus at AGO P2 and P3 in relation to solar wind and magnetospheric drivers. Specifically, we investigate solar wind dynamic pressure, IMF B_z, substorms (as indicated by the *AE* index and geosynchronous particle injections), and the K_p index. First three case studies are presented that encapsulate general trends seen in the data, and this is followed by a statistical analysis of the entire data set.

[23] The *AE* and K_p indices are taken from the World Data Center for Geomagnetism, Kyoto. The solar wind data are from the WIND spacecraft and taken from the high time resolution OMNIWeb database which provides 1 min resolution solar wind data propagated to the Earth's bow shock nose. We also use energetic particle data taken from the SOPA instrument [*Belian et al.*, 1992] operating on board the LANL 1994-084, LANL-97A and 1989-046 spacecraft. The SOPA instruments measure the energetic electron flux from 50 keV to 2 MeV, but we show only the 3 lowest-energy channels (50–74, 74–110, 110–160 keV) since only particles in this energy range are expected to contribute to the growth of chorus waves.

[24] The first case study illustrates the observation of chorus during a period of low geomagnetic and solar wind activity on 24 February 2007 (Figure 4). During this interval, the IMF B_z is weakly positive, the dynamic pressure is low,

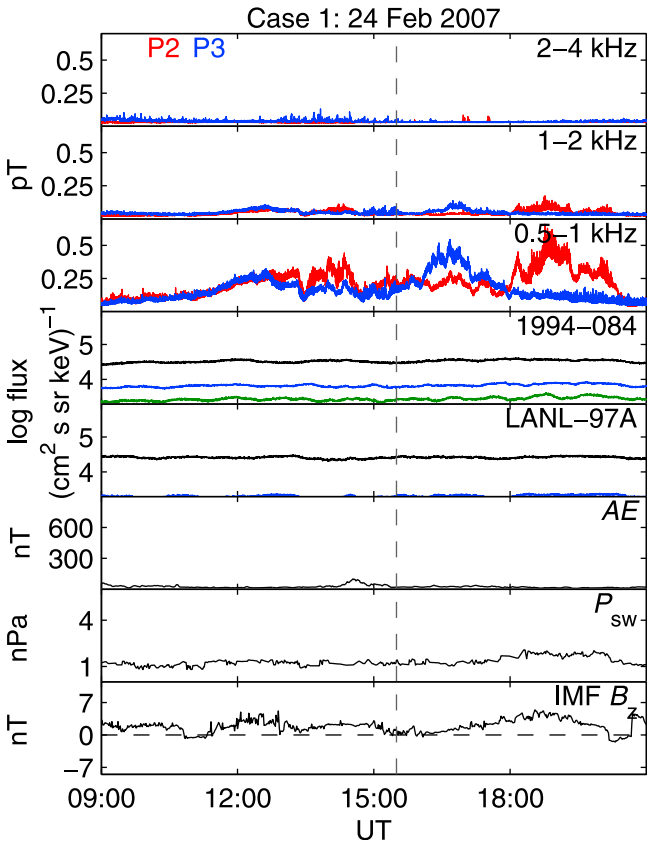

Figure 4. Case study 1 on 24 February 2007. The first, second, and third panels are the three lowest-frequency channels of the ELF/VLF system for P2 (red) and P3 (blue). Next are the three lowest-energy channels of the SOPA energetic electron detectors for LANL spacecraft 1994-084 (fourth panel) and LANL-97A (fifth panel). The black line is the 50–74 keV channel, the blue is 74–110 keV, and the green is 110–160 keV. The sixth panel is the *AE* index. The seventh and eighth panels are the solar wind dynamic pressure and the IMF B_z convected to the bow shock. The mapped locations of the ground stations and the LANL spacecraft at 1530 UT (dashed vertical line) are shown in Figure 5 (left).

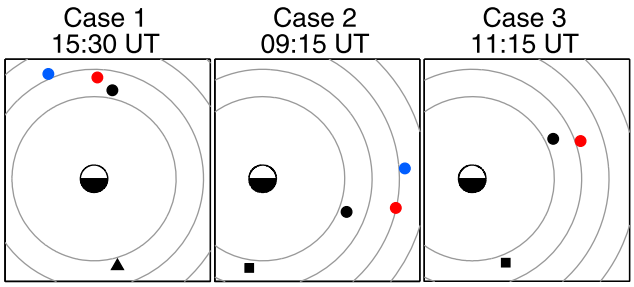

Figure 5. The mapped locations of P2 (red) and P3 (blue) along with the locations of the LANL spacecraft 1994-084 (black circle), LANL-97A (black triangle), and 1989-046 (black square) are shown in the GSM equatorial plane at selected times for each of the three case studies (vertical lines in Figures 4, 6, and 7). The concentric circles are located at 6, 8, 10, and 12 R_E.

and no substorms are observed as indicated by the low values of *AE* and an absence of energetic particle injections observed by the SOPA instruments at geosynchronous orbit. The location of the ground stations and the LANL spacecraft mapped to the GSM equatorial plane at 1530 UT are shown in Figure 5 (left). Despite the low geomagnetic activity, chorus is clearly observed at both AGO P2 and P3. The onset of chorus activity on this day is gradual and by ~8 MLT (1130 UT) the amplitude exceeds 0.16 pT in the 0.5–1 kHz channel. Early in the event interval, the amplitudes at the two stations track one another, but later amplitude intensifications occur separately at the two stations. From 1600–1800 UT, the amplitude at P3 exceeds that of P2 and also exceeds the mean event amplitudes (Figure 3b) at those particular local times.

[25] The second case example shows the onset of chorus in response to substorm activity on 6 March 2007 (Figure 6). At 0928 UT, LANL spacecraft 1989-046 observes an energetic electron injection in the midnight local time sector (2340 MLT (see Figure 5, middle)). Within ~10 min, the electron injection is observed by 1994-084 (~5 MLT). Correspondingly, AGO P2 observes a prompt onset of chorus as the anisotropic electron distributions drift past the local time of the station (~6 MLT). A subsequent substorm associated electron injection at 1150 UT also results in a prompt chorus onset with the double peaked electron signature observed by 1989-046 mirrored in the two chorus peaks seen at AGO P2. After the second substorm, the magnetosphere undergoes a period of quietening as the IMF turns strongly northward and no further substorm activity is observed (although the SOPA instruments continue to measure enhanced energetic electron fluxes as compared to Figure 4). As AGO P2 rotates to the noon sector, very intense chorus activity is observed. Activity at P3 mirrors that of P2 although wave amplitudes at P3 are substantially lower (with the exception of the first substorm injection).

[26] The final case example demonstrates the absence of chorus after a substorm injection. On 23 March 2007, two distinct substorms occur at ~1125 and ~1425 UT as seen in peaks in the *AE* index and associated energetic electron injections at geosynchronous orbit (Figure 7). Similar to the previous case example, for the first substorm injection, a prompt onset of chorus is seen. AGO P3 observes intense auroral hiss on this day and thus is not shown. In contrast, for the second substorm, no chorus is observed at AGO P2. It is interesting to note that the second substorm is larger than the first in terms of both the peak *AE* value and higher geosynchronous electron fluxes.

[27] It is possible that the absence of chorus in response to the second electron injection is due to the lack of a propagation path to the ground. Another possibility is that there may be a local time dependence of the chorus driver. In both case 2 and case 3, chorus onset in response to the substorm occurred when the stations were just postdawn (6–9 MLT). While when the stations were near noon, the waves were not necessarily driven by substorms (case 3) and can be observed during periods of low geomagnetic and solar wind driving (case 1 and 2). Also, the wave amplitude observed at P3 only considerably exceeded that of P2 during the quietest geomagnetic conditions (case 1 in which the P3 amplitude was nearly double that of P2 for over an hour).

5. Wave Drivers: Statistics

[28] To further investigate the trends suggested in the case studies, we perform a statistical analysis of wave occurrence probability as a function of solar wind and geomagnetic conditions. Figure 8 shows the normalized occurrence probability for a chorus event with various levels of K_p (Figure 8a), *AE** (Figure 8b), IMF B_z (Figure 8c), solar wind

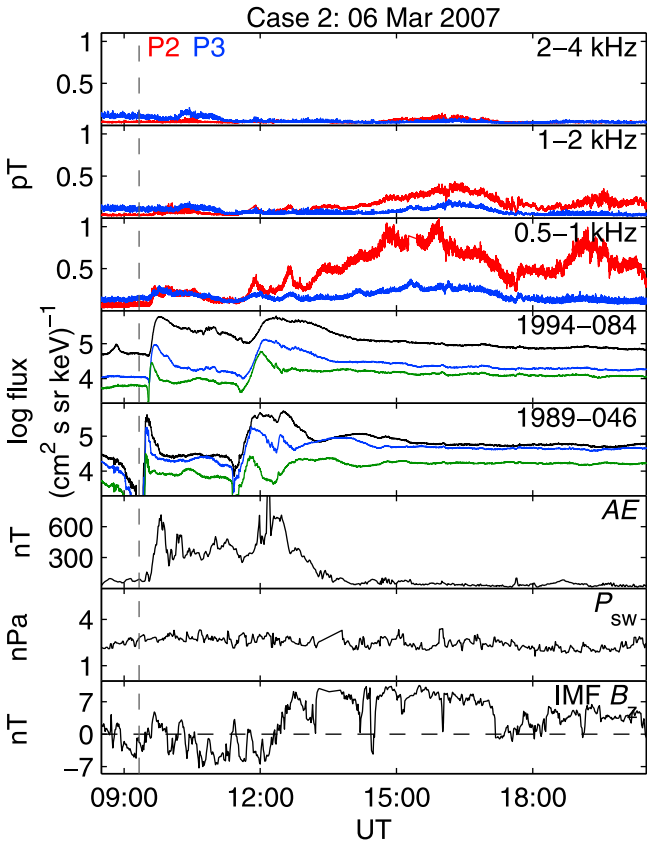

Figure 6. Same as Figure 4 for case 2 on 6 March 2007.

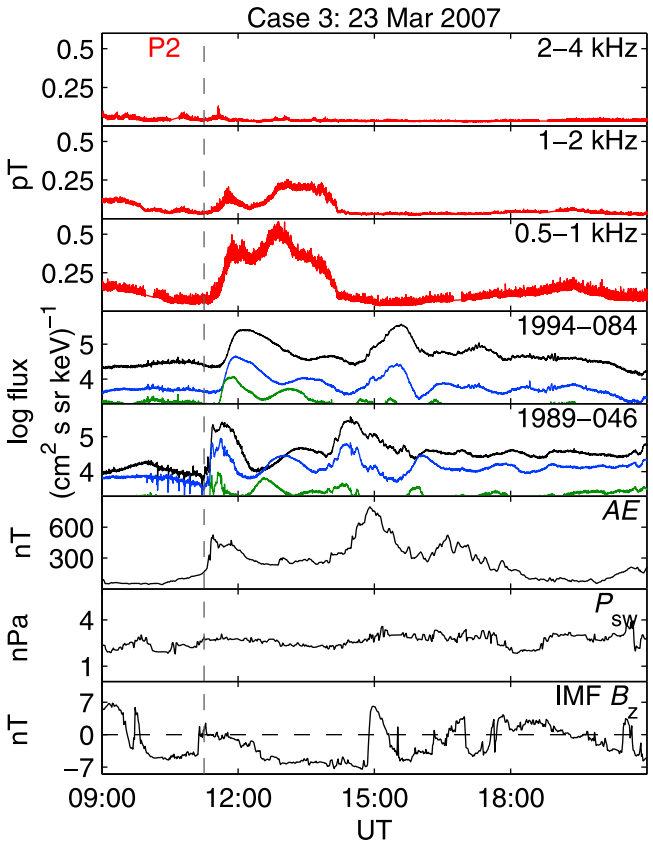

Figure 7. Same as Figure 4 for case 3 on 23 March 2007. P3 observed intense dayside hiss on this day and is therefore not shown.

pressure (P_{sw}) (Figure 8d), and change in solar wind dynamic pressure (ΔP_{sw}) (Figure 8e). For K_p, B_z, and P_{sw}, we examine the median value of each variable during the chorus event interval. For *AE**, we take the 95th percentile value of the *AE* index over the previous 3 h. Since substorms are inherently impulsive events, a maximum value of *AE* is preferred over a median value. However, in order to avoid data spikes, a 95th percentile value is used rather than the absolute maximum. Also, a 3 h window is used for *AE** in order to account for the magnetic and electric drifts of the source electrons. Finally, we examine ΔP_{sw} by subtracting the maximum value from the minimum value for the event interval with a negative value meaning the maximum pressure value occurred before the minimum in time.

[29] The normalized occurrence probability is further divided by local time. The black bars in Figure 8 are the normalized occurrence probabilities for the entire dayside chorus window (5.5–18.5 MLT), the light gray are for MLT < 10 (dawn sector) and the white are for MLT > 10 (noon sector). The mapped location of the stations when they are located at 10 MLT in the ionosphere is indicated by the square symbol in Figure 2. The mapped location is slightly west of 10 MLT in the equatorial plane since field lines in flanks are pulled tailward by the solar wind flow past the magnetosphere. Also, we show the normalized probabilities combined for both stations since the trends for each variable are essentially identical albeit with P3 having slightly lower probabilities.

[30] In order to calculate the normalized occurrence probabilities, we first calculate the activity level for all variables for each 30 min interval for which there is valid AGO data available. Each variable is then divided into four activity level ranges such that each range contains an equal number of intervals over all days and at all local times. This is done in order to minimize the error associated with the

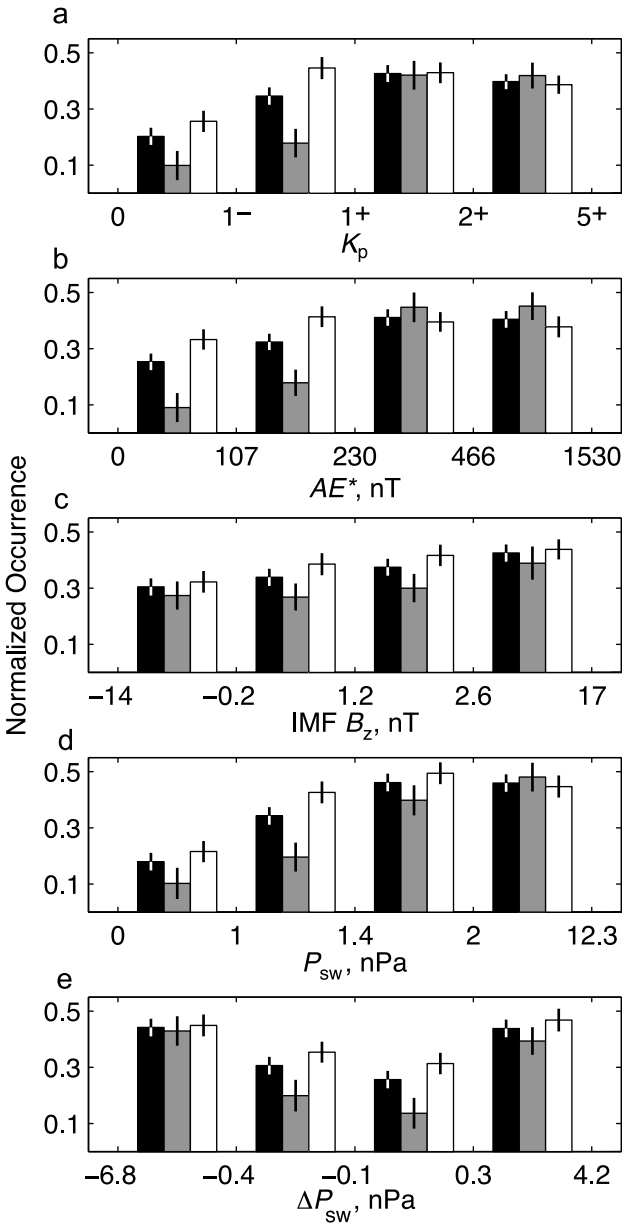

Figure 8. Normalized chorus event occurrence as a function of (a) K_p, (b) *AE**, (c) IMF B_z, (d) solar wind pressure P_{sw}, and (e) change in solar wind pressure ΔP_{sw}. Black bars are all dayside chorus events, gray bars are events with MLT < 10 (dawn sector events), and white bars are events with MLT > 10 (noon sector events). Vertical lines at the top of each bar indicate the estimated error in the occurrence probability.

normalized occurrence probability although it does also result in somewhat usual binning of the activity levels. Next, the probability of a chorus event occurring within each range of the activity level is calculated ("event probability") as well as the probability of each range of activity occurring ("activity probability"). This is done separately for each local time range (entire dayside, dawn sector, and noon sector). For the bars showing the entire dayside, the activity probability is always 0.25 by design, and for breakdown into the dawn and noon sectors, it is close to 0.25 though it may not be identically so depending on the variation of magnetic activity over the study interval. The normalized occurrence probability for chorus is then the event probability divided by the activity probability. The error associated with each normalized occurrence probability is related to the number of times (N) the activity measure is within a given range (numerator in the activity probability). Since random fluctuations are expected to be on the order of $\sqrt{N}$, we estimate the error in the normalized occurrence probability as $\frac{\sqrt{N}}{N}$. The minimum (maximum) value of N for all activity measures and local time ranges in Figure 8 is 288 (1014), and thus the maximum (minimum) error in the normalized chorus event probability is ±0.06 (±0.03).

[31] As shown in Figure 8, the overall trend for the K_p and AE^* indices are similar, and specifically, we find a strong local time dependence. Waves in the dawn local time are significantly more likely to occur during periods of enhanced geomagnetic activity. For example, waves at dawn occur only at a rate of 0.09 ± 0.05 when $AE^* < 107$ nT but at a rate of 0.45 ± 0.05 when $AE^* \geq 466$ nT. On the other hand, waves near noon appear to be relatively independent of geomagnetic activity with the normalized occurrence for $AE^* > 107$ nT and $K_p > 1^-$ having values that are well within the range of one error bar. Further, even for the lowest activity level, waves are 3.7 times more likely near noon than near dawn for $AE^* \leq 107$ nT and 2.6 times more likely for $K_p \leq 1^-$. Thus, a primary conclusion from this analysis is that in the outer magnetosphere on the dawn side, chorus is primarily driven by substorm electron injections while in the noon sector wave growth occurs both during quiet as well as active conditions.

[32] There is a trend for waves to be slightly more likely with increasingly positive values of IMF B_z. For example for the entire dayside, waves occur at a rate of 0.3 when $B_z < -0.2$ nT while at a rate of 0.42 when $B_z \geq 2.6$ nT. The difference between the probabilities is four times the estimated error (±0.03 for both), so we consider this to be a statistically significant trend. There does not appear to be a local time dependence associated with B_z.

[33] Waves across the entire dayside are more likely when solar wind dynamic pressure is higher. The overall occurrence rate is 0.18 ± 0.03 when the pressure is <1 nPa but increases to 0.46 ± 0.03 when pressure is ≥2 nPa. Further, waves are more sensitive to dynamic pressure in the dawn sector than in the noon sector. For instance, waves near dawn are 4–5 times more likely at higher pressure ($P_{sw} \geq 2$) than lower ($P_{sw} < 1$) while waves near noon are only about 2 times more likely. In terms of changes in dynamic pressure, waves across the entire dayside are more likely for both increases ($\Delta P_{sw} > 0.3$) and decreases ($\Delta P_{sw} \leq -0.4$) in pressure. Again, waves at dawn are slightly more sensitive to pressure changes with waves at dawn being 1.5–2 times more likely during pressure changes while waves at noon are only 0.25–0.5 times more likely.

[34] As mentioned in section 3, the event amplitudes at P2 are higher than at P3 ~80% of the time. Case study 1 showed an interesting example when, during a period of low geomagnetic activity, the amplitude at P3 exceeded that of P2 for a few hours. We examined all such intervals and found a similar trend. The normalized probability of occurrence for events when the amplitude at P3 exceeds that of P2 is 0.39 ± 0.03 when $AE^* < 230$ nT whereas it is 0.29 ± 0.03 when $AE^* \geq 230$ nT. A value of 230 nT was selected since it is the median value of AE^* for the entire study interval. Thus, the event amplitude at P3 (the higher-latitude station) is more likely to exceed that of P2 during quiet intervals than during active intervals.

6. Discussion

[35] We have analyzed wave data from two high invariant latitude ground stations and explored the variability of chorus (discrete rising emission tones together with unstructured hiss) occurrence in terms of solar wind and magnetospheric drivers. Both stations observe chorus in a broad window of local time across the dayside when the stations are on closed magnetic field lines. Wave occurrence rates rise rapidly from ~0.06–0.12 at dawn to their maximum value of ~0.5–0.6 near local noon. That is, ~50–60% of 30 min intervals near noon have a median chorus amplitude of at least 0.16 pT. Occurrence probabilities at P2 are consistently higher than P3 with the average difference in the rate being 0.15. Further, the probability of observing a chorus event on any given day (i.e., a chorus event in at least one 30 min interval) is 0.83 at P2 and 0.74 at P3. The event amplitudes also peak near noon, and ~80% of the time event amplitudes are larger at P2 than P3. For event intervals when the amplitude of P3 exceeds that of P2, the geomagnetic conditions are more likely to be quiet.

[36] In examining the magnetospheric and solar wind drivers of the waves, we find an interesting local time effect. When the stations are in the dawn local time sector ($5.5 < MLT < 10$), the onset of waves is clearly linked to substorms, as seen by the AE index as well as by energetic electron injections observed at geosynchronous orbit. However, as the stations rotate to noon ($MLT > 10$), wave occurrence rates are higher and appear to be relatively independent of geomagnetic activity as measured by K_p and AE. As also seen in the case studies, chorus near noon at times appears related to substorm activity, but intense waves can also be observed during extended quiet periods. Waves across the entire dayside are more likely during higher solar wind dynamic pressure as well as during significant changes in pressure. However, the occurrence of waves at dawn is slightly more sensitive to pressure. That is, there is a bigger difference in occurrence probability between low pressure and high pressure at dawn than at noon.

[37] Substorm associated chorus is a relatively well-understood phenomenon [e.g., *Tsurutani and Smith*, 1974; *Burtis and Helliwell*, 1976; *Smith et al.*, 1999]. High fluxes of electrons injected from the magnetotail are preferentially heated in the perpendicular direction resulting in anisotropic populations which are unstable to wave growth.

[38] Our finding that waves in the outer magnetosphere near noon are not confined to substorm intervals is consistent with past reports by *Tsurutani and Smith* [1977] and *Li et al.* [2009] who showed that the waves in this region have a high probability of occurrence and can persist during quiet intervals. Favorable conditions for wave growth exist in the outer dayside magnetosphere for a number of reasons. First, solar wind compression of the dayside magnetosphere results in L shell splitting of electrons drifting from dawn toward noon [e.g., *Roederer*, 1967; *West et al.*, 1973]. Drift shell splitting ensures that the most anisotropic distributions will be located at large radial distances in the noon sector. Enhanced solar wind dynamic pressure will further enhance drift shell splitting and increase the anisotropy on the dayside contributing to higher wave occurrence such as reported here. During geomagnetically quiet conditions, the fluxes of source electrons (5–150 keV) are likely to be relatively low throughout the magnetosphere. However, weak convection may continue in the outer magnetosphere as a result of viscous interaction or poleward of the cusp reconnection [e.g., *Förster et al.*, 2008]. Thus, a narrow flow channel in the outer magnetosphere would bring plasma sheet electrons to the dayside and drift shell splitting may result in unstable distributions close to the magnetopause.

[39] *Tsurutani and Smith* [1977] suggested that the off-equatorial minimum-B pockets on the dayside could be a favorable region for wave growth. The location of the minimum-B pockets with respect to the viewing area of the stations as estimated by the T01 magnetic field model is shown in Figure 2. The color coding indicates the latitude of the minimum magnetic field value along a field line that crosses the equator at that point. Throughout the inner magnetosphere, the minimum magnetic field value lies at $\lambda \approx 0°$ as would be expected from a dipole field, but on the dayside close to the magnetopause, solar wind pressure distorts the dipole and moves the minimum-B location to higher latitudes. We note that all magnetic field models that include external sources have minimum-B pockets, but the exact size and shape of the region depends highly on the field model used as well as the solar wind parameters and the dipole tilt angle. For the specific conditions considered here (T01 model, $P_{sw} = 3$ nPa, $B_z = 2$ nT, zero dipole tilt), the off-equatorial minimum-B region has a radial extent of ~1.7 R_E at noon and an azimuthal extent of ~6 h of MLT. As the observing stations rotate from the dawn to noon sector, the ELF/VLF viewing areas of the two stations begin to include the off-equatorial minimum-B regions. Thus, it is possible that a significant fraction of the noon sector waves observed at the ground stations have originated in the minimum-B pockets.

[40] Energetic electrons drifting eastward from dawn have access to the minimum-B pockets through so-called "Shabansky orbits" [*Shabansky*, 1971], more recently referred to as drift shell bifurcation [*Öztürk and Wolf*, 2007]. Drift shell bifurcation is a nonadiabatic process (the second invariant is violated) by which [*Öztürk and Wolf*, 2007, paragraph 1] particles "with equatorial pitch angles sufficiently close to 90° will cross the dayside not along an equatorial path, but along one of the two branches (of low magnetic field) on either side of the equatorial plane." The two branches rejoin in the postnoon sector, and the bounce centers return to the equatorial plane. It is unclear whether the drift shell bifurcation process additionally modifies the electron distribution or just acts to move the energetic electrons (and wave generation region) off the equator. The location of the minimum-B is important for wave-particle interactions since it is here that resonant energies are minimized and pitch angle anisotropies are maximized, both of which favor wave growth.

[41] Previous studies have reported high fluxes of energetic electrons in the minimum-B pockets in the aftermath of substorms [e.g., *Antonova and Nikolaeva*, 1979]. *Tsurutani et al.* [2009] noted that wave generation in the minimum-B pockets could result from freshly injected substorm electrons or alternatively increases in solar wind dynamic pressure could increase the anisotropy of the existing electron population through betatron acceleration. Our findings and past work [*Gail et al.*, 1990; *Salvati et al.*, 2000] support the idea that pressure increases lead to enhanced wave growth. In this study, it was found that pressure decreases were also associated with chorus events. However, it is likely that the chorus was associated with earlier intervals of higher pressure rather than the pressure decrease itself.

[42] There is an additional effect of magnetic field geometry in the outer noon sector region that may further contribute to favorable conditions for wave growth. The trapping of electrons in the potential well of the wave is considered a necessary condition for nonlinear wave growth [*Dowden et al.*, 1978; *Bell and Inan*, 1981; *Omura et al.*, 1991]. The conditions for particle trapping depend in part on the degree to which the strength of the magnetic field changes along the field line ($\frac{dB}{ds}$) with smaller values of $\frac{dB}{ds}$ favoring trapping and thus wave growth [e.g., *Nunn*, 1974; *Omura et al.*, 1991]. This effect may contribute to the difference in the latitudinal extent of dayside and nightside chorus with nightside chorus being more closely confined to the equator [e.g., *Meredith et al.*, 2001]. On the nightside, magnetotail currents tend to stretch the magnetic field lines, and thus B varies more rapidly with latitude. On the other hand, solar wind compression of the magnetic field on the dayside results in field lines having low values of $\frac{dB}{ds}$ over a wider range of latitudes around the equator.

[43] A region of maximum homogeneity of the magnetic field (small $\frac{dB}{ds}$) is found in the outer noon sector magnetosphere. Figure 9 shows the strength of the magnetic field at noon as function of latitude for a set of field lines that cross the equatorial plane at radial distances from 6.0 to 9.0 R_E using the T01 model and the same parameters as Figure 2. For the innermost field line crossing the equator at 6.0 R_E, the minimum magnetic field value (black dot) is near 0° latitude but by ~±7° the field has increased by 5% of the minimum. Moving outward, the field varies more slowly with latitude such that at 8.0 R_E, the minimum-B has moved off the equator, but the value of the field stays within 5% of the minimum value over a range of ~±22°. Closer to the magnetopause, $\frac{dB}{ds}$ again changes more rapidly with latitude. We assert that this region of maximum homogeneity of the magnetic field that occurs in the transition region from equatorial to off-equatorial minimum-B may be particularly favorable for wave generation since an important condition for nonlinear wave growth is met over a wide range of latitude. The viewing area of the AGO stations P2 and P3

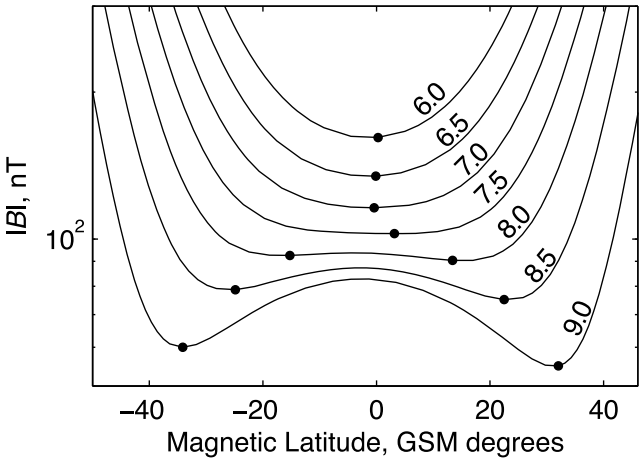

Figure 9. The strength of the magnetic field as a function of latitude for a set of field lines that cross the equatorial plane at noon at radial distances from 6.0 to 9.0 R_E using the T01 magnetic field model. The dots indicate the location of the local minimum in the magnetic field strength.

encompass this region, a likely contributor to the high wave occurrence probabilities seen in the noon sector.

[44] There are interesting differences between the two stations despite being separated in latitude by only 2° with the higher-latitude station, P3, having lower occurrence rates and event amplitudes. Although, the T01 magnetic field model maps P3 onto closed field lines for conditions examined here, it is possible that the poleward edge of the field of view and at times the station itself lies under open field lines. Even if the entire viewing area of P3 does map to closed field lines, it is possible that the wave generation region is often equatorward of the station, and thus only waves that have propagated from lower latitudes in the Earth-ionosphere waveguide would be observed and correspondingly at reduced amplitudes. This may be the case in the hours close to local dawn, where the occurrence rates at P2 and P3 are fairly similar, but the event amplitudes at P3 are consistently lower. Also in the noon sector, the process of drift shell bifurcation has only been studied under nonvarying field conditions [e.g., *Öztürk and Wolf*, 2007], and changes in the field resulting from solar wind pressure or IMF variations could destabilize these drift orbits close to the magnetopause. Energetic electrons entering the off-equatorial minimum-B pockets could be rapidly lost to the cusp, precluding wave generation near noon in the region closest to the magnetopause boundary [e.g., *Shao et al.*, 2005]. The discussion above is consistent with the finding that during the intervals when the event amplitude at P3 exceeds that of P2, the geomagnetic conditions are more likely to be quiet, and thus the magnetosphere is inflated on the dayside. Finally, the difference between the occurrence rate at the two stations (0.15 on average) may suggest that the actual ELF/VLF viewing area of the stations is smaller than that depicted in Figure 2.

[45] The peak in wave amplitudes in the prenoon sector at P2 is consistent with reports by *Tsurutani and Smith* [1977] and *Li et al.* [2009]. However, since our observations are from ground-based stations, we cannot discount possible propagation effects. Chorus in the dawn sector is likely generated near the equatorial plane whereas near noon the waves are likely generated in an extended region of latitude around the equator or in the high-latitude minimum-B pockets. Thus, the propagation from the source region to the ionosphere may be significantly shorter at noon than dawn. Specifically, the T01 field model indicates that the length of the field line from the minimum-B location to the ionosphere can be ~40% shorter at noon than at dawn. The longer propagation paths at dawn could result in more significant Landau damping prior to the waves reaching the ionosphere [e.g., *Bortnik et al.*, 2007]. In addition, nonducted propagation effects may allow more efficient penetration of waves from the equatorial region down to low altitudes near noon as compared with dawn, but these effects require further study. Thus, at this point we cannot determine whether the reduced amplitudes near dawn solely result from differences in the wave amplitudes in the source region or are a result of propagation effects.

7. Summary

[46] The Antarctic plateau provides a unique window for routine remote sensing of dynamic processes occurring in the Earth's magnetosphere. Here we have analyzed ELF/VLF data collected by two remote, autonomous, high-latitude ($\Lambda = -69.8°, -71.8°$) ground stations, and reported on the occurrence rate, amplitude, and drivers of magnetospheric chorus events. Chorus is observed in a broad window of local time when the stations are on closed field lines on the dayside. We find that chorus observed in the dawn sector ($5.5 < \mathrm{MLT} < 10$) is associated with disturbed geomagnetic conditions, specifically substorm electron injections and intervals of enhanced solar wind dynamic pressure. As the stations rotate toward noon (MLT > 10), wave occurrence rates rapidly increase to ~0.50–0.60. In addition, noon sector waves are less dependent on geomagnetic activity with the waves at times being associated with substorms but also observed relatively often during quiet conditions.

[47] The noon sector outer magnetosphere may be particularly conducive to wave growth over a range of geomagnetic conditions for several reasons. Solar wind compression of the dayside magnetosphere results in shell splitting of the eastward drifting source electrons, forming highly anisotropic distributions in the outer noon sector. Consequently, we observe noon sector waves nearly twice as often when the solar wind pressure is ≥2 nPa. Further, the compression of the field creates a region over which the strength of the magnetic field is nearly constant for ~±10–20° of magnetic latitude around the equator. Since nonlinear wave growth rates depend on the homogeneity of the magnetic field, the region ~1.5–3 R_E inward of the magnetopause may be a preferred region for wave growth. These two factors likely result in the high occurrence of dayside chorus as observed here and reported elsewhere [*Tsurutani and Smith*, 1977; *Koons and Roeder*, 1990; *Li et al.*, 2009]. In addition, wave growth rates may fall off in region closer to the magnetopause, as suggested by the lower occurrence probability and amplitude of chorus events at the higher-latitude station.

[48] **Acknowledgments.** This work was supported by the National Science Foundation under grants 0341165, 0636927, and 0524825.

[49] Zuyin Pu thanks O Santolik and Gary A. Abel for their assistance in evaluating this paper.

References

Abel, G. A., M. P. Freeman, A. J. Smith, and G. D. Reeves (2006), Association of substorm chorus events with drift echoes, *J. Geophys. Res.*, *111*, A11220, doi:10.1029/2006JA011860.

Antonova, A. E., and N. S. Nikolaeva (1979), Energetic electron fluxes in the Earth's upper magnetosphere from Prognoz-3 observations, *Geomagn. Aeron.*, *19*, 615–622.

Belian, R. D., G. R. Gisler, T. Cayton, and R. Christensen (1992), High-Z energetic particles at geosynchronous orbit during the great solar proton event series of October 1989, *J. Geophys. Res.*, *97*, 16,897–16,906.

Bell, T. F., and U. S. Inan (1981), Transient nonlinear pitch angle scattering of energetic electrons by coherent VLF wave packets in the magnetosphere, *J. Geophys. Res.*, *86*, 9047–9063.

Bortnik, J., R. M. Thorne, and N. P. Meredith (2007), Modeling the propagation characteristics of chorus using CRRES suprathermal electron fluxes, *J. Geophys. Res.*, *112*, A08204, doi:10.1029/2006JA012237.

Burtis, W. J., and R. A. Helliwell (1976), Magnetospheric chorus: Occurrence patterns and normalized frequency, *Planet. Space Sci.*, *24*, 1007–1007.

Burton, R. K., and R. E. Holzer (1974), The origin and propagation of chorus in the outer magnetosphere, *J. Geophys. Res.*, *79*, 1014–1023.

Chum, J., and O. Santolík (2005), Propagation of whistler-mode chorus to low altitudes: Divergent ray trajectories and ground accessibility, *Ann. Geophys.*, *23*, 3727–3738.

Cornilleau-Wehrlin, N., R. Gendrin, F. Lefeuvre, M. Parrot, R. Grard, D. Jones, A. Bahnsen, E. Ungstrup, and W. Gibbons (1978), VLF electromagnetic waves observed onboard GEOS-1, *Space Sci. Rev.*, *22*, 371–382.

Dowden, R. L., A. D. McKay, L. E. S. Amon, H. C. Koons, and M. H. Dazey (1978), Linear and nonlinear amplification in the magnetosphere during a 6.6-kHz transmission, *J. Geophys. Res.*, *83*, 169–181.

Förster, M., S. E. Haaland, G. Paschmann, J. M. Quinn, R. B. Torbert, H. Vaith, and C. A. Kletzing (2008), High-latitude plasma convection during northward IMF as derived from in-situ magnetospheric cluster EDI measurements, *Ann. Geophys.*, *26*, 2685–2700.

Gail, W. B., U. S. Inan, R. A. Helliwell, and D. L. Carpenter (1990), Gyroresonant wave-particle interactions in a dynamic magnetosphere, *J. Geophys. Res.*, *95*, 15,103–15,112.

Gurnett, D. A., and B. J. O'Brien (1964), High-latitude geophysical studies with satellite Injun 3, 5, very low frequency electromagnetic radiation, *J. Geophys. Res.*, *69*, 65–89.

Helliwell, R. A. (1965), *Whistlers and Related Ionospheric Phenomena*, Stanford Univ. Press, Stanford, Calif.

Horne, R. B., et al. (2005), Wave acceleration of electrons in the Van Allen radiation belts, *Nature*, *437*, 227–230.

Inan, U. S., Y. T. Chiu, and G. T. Davidson (1992), Whistler-mode chorus and morningside aurorae, *Geophys. Res. Lett.*, *19*, 653–656.

Koons, H. C., and J. L. Roeder (1990), A survey of equatorial magnetospheric wave activity between 5 and 8 R(E), *Planet. Space Sci.*, *38*, 1335–1341.

LaBelle, J., A. T. Weatherwax, J. Perring, E. Walsh, M. L. Trimpi, and U. S. Inan (1998), Low-frequency impulsive auroral hiss observations at high geomagnetic latitudes, *J. Geophys. Res.*, *103*, 20,459–20,468.

Lauben, D. S., U. S. Inan, T. F. Bell, and D. A. Gurnett (2002), Source characteristics of ELF/VLF chorus, *J. Geophys. Res.*, *107*(A12), 1429, doi:10.1029/2000JA003019.

LeDocq, M. J., D. A. Gurnett, and G. B. Hospodarsky (1998), Chorus source locations from VLF Poynting flux measurements with the Polar spacecraft, *Geophys. Res. Lett.*, *25*, 4063–4066.

Li, W., R. M. Thorne, V. Angelopoulos, J. Bortnik, C. M. Cully, B. Ni, O. LeContel, A. Roux, U. Auster, and W. Magnes (2009), Global distribution of whistler-mode chorus waves observed on the THEMIS spacecraft, *Geophys. Res. Lett.*, *36*, L09104, doi:10.1029/2009GL037595.

Lorentzen, K. R., J. B. Blake, U. S. Inan, and J. Bortnik (2001), Observations of relativistic electron microbursts in association with VLF chorus, *J. Geophys. Res.*, *106*, 6017–6028.

Masson, A., et al. (2009), Advances in plasmaspheric wave research with CLUSTER and IMAGE observations, *Space Sci. Rev.*, *145*, 137–191.

Meredith, N. P., R. B. Horne, and R. R. Anderson (2001), Substorm dependence of chorus amplitudes: Implications for the acceleration of electrons to relativistic energies, *J. Geophys. Res.*, *106*, 13,165–13,178.

Nunn, D. (1974), A self-consistent theory of triggered VLF emissions, *Planet. Space Sci.*, *22*, 349–378.

O'Brien, T. P., M. D. Looper, and J. B. Blake (2004), Quantification of relativistic electron microburst losses during the GEM storms, *Geophys. Res. Lett.*, *31*, L04802, doi:10.1029/2003GL018621.

Omura, Y., H. Matsumoto, D. Nunn, and M. J. Rycroft (1991), A review of observational, theoretical and numerical studies of VLF triggered emissions, *J. Atmos. Terr. Phys.*, *53*, 351–368.

Öztürk, M. K., and R. A. Wolf (2007), Bifurcation of drift shells near the dayside magnetopause, *J. Geophys. Res.*, *112*, A07207, doi:10.1029/2006JA012102.

Parrot, M., O. Santolík, N. Cornilleau-Wehrlin, M. Maksimovic, and C. Harvey (2003), Magnetospherically reflected chorus waves revealed by ray tracing with CLUSTER data, *Ann. Geophys.*, *21*, 1111–1120.

Pope, J. H. (1960), Effect of latitude on the diurnal maximum of 'dawn chorus,' *Nature*, *185*, 87–88.

Roederer, J. G. (1967), On the adiabatic motion of energetic particles in a model magnetosphere, *J. Geophys. Res.*, *72*, 981–992.

Salvati, M. A., U. S. Inan, T. J. Rosenberg, and A. T. Weatherwax (2000), Solar wind control of polar chorus, *Geophys. Res. Lett.*, *27*, 649–652.

Santolík, O., D. A. Gurnett, J. S. Pickett, M. Parrot, and N. Cornilleau-Wehrlin (2003), Spatio-temporal structure of storm-time chorus, *J. Geophys. Res.*, *108*(A7), 1278, doi:10.1029/2002JA009791.

Santolík, O., D. A. Gurnett, J. S. Pickett, M. Parrot, and N. Cornilleau-Wehrlin (2005a), Central position of the source region of storm-time chorus, *Planet. Space Sci.*, *53*, 299–305.

Santolík, O., E. Macúšová, K. H. Yearby, N. Cornilleau-Wehrlin, and H. S. K. Alleyne (2005b), Radial variation of whistler-mode chorus: first results from the STAFF/DWP instrument on board the Double Star TC-1 spacecraft, *Ann. Geophys.*, *23*, 2937–2942.

Santolík, O., J. Chum, M. Parrot, D. A. Gurnett, J. S. Pickett, and N. Cornilleau-Wehrlin (2006), Propagation of whistler mode chorus to low altitudes: Spacecraft observations of structured ELF hiss, *J. Geophys. Res.*, *111*, A10208, doi:10.1029/2005JA011462.

Sazhin, S. S., and M. Hayakawa (1992), Magnetospheric chorus emissions—A review, *Planet. Space Sci.*, *40*, 681–697.

Sazhin, S. S., K. Bullough, and M. Hayakawa (1993), Auroral hiss: A review, *Planet. Space Sci.*, *41*, 153–166.

Shabansky, V. P. (1971), Some processes in the magnetosphere, *Space Sci. Rev.*, *12*, 299–418.

Shao, X., S. F. Fung, L. C. Tan, K. Papadopoulos, M. Wiltberger, and M. C. Fok (2005), Investigation of 3D energetic particle transport inside quiet-time magnetosphere using particle tracing in global MHD model, in *The Inner Magnetosphere: Physics and Modeling*, *Geophys. Monogr. Ser.*, vol. 155, edited by T. I. Pulkkinen, N. A. Tsyganenko, and R. H. W. Friedel, pp. 307–318, AGU, Washington, D. C.

Smith, A. J., M. P. Freeman, M. G. Wickett, and B. D. Cox (1999), On the relationship between the magnetic and VLF signatures of the substorm expansion phase, *J. Geophys. Res.*, *104*, 12,351–12,360.

Smith, R. L., R. A. Helliwell, and I. W. Yabroff (1960), A theory of trapping of whistlers in field-aligned columns of enhanced ionization, *J. Geophys. Res.*, *65*, 815–823.

Sonwalkar, V. S., and J. Harikumar (2000), An explanation of ground observations of auroral hiss: Role of density depletions and meter-scale irregularities, *J. Geophys. Res.*, *105*, 18,867–18,884.

Summers, D., B. Ni, and N. P. Meredith (2007), Timescales for radiation belt electron acceleration and loss due to resonant wave-particle interactions: 2. Evaluation for VLF chorus, ELF hiss, and electromagnetic ion cyclotron waves, *J. Geophys. Res.*, *112*, A04207, doi:10.1029/2006JA011993.

Thorne, R. M., S. R. Church, W. J. Malloy, and B. T. Tsurutani (1977), The local time variation of ELF emissions during periods of substorm activity, *J. Geophys. Res.*, *82*, 1585–1590.

Tsuruda, K., S. Machida, T. Terasawa, A. Nishida, and K. Maezawa (1982), High spatial attenuation of the Siple transmitter signal and natural VLF chorus observed at ground-based chain stations near Roberval, Quebec, *J. Geophys. Res.*, *87*, 742–750.

Tsurutani, B. T., and E. J. Smith (1974), Postmidnight chorus: A substorm phenomenon, *J. Geophys. Res.*, *79*, 118–127.

Tsurutani, B. T., and E. J. Smith (1977), Two types of magnetospheric ELF chorus and their substorm dependences, *J. Geophys. Res.*, *82*, 5112–5128.

Tsurutani, B. T., O. P. Verkhoglyadova, G. S. Lakhina, and S. Yagitani (2009), Properties of dayside outer zone chorus during HILDCAA events: Loss of energetic electrons, *J. Geophys. Res.*, *114*, A03207, doi:10.1029/2008JA013353.

Tsyganenko, N. A. (2002a), A model of the near magnetosphere with a dawn-dusk asymmetry: 1. Mathematical structure, *J. Geophys. Res.*, *107*(A8), 1179, doi:10.1029/2001JA000219.

Tsyganenko, N. A. (2002b), A model of the near magnetosphere with a dawn-dusk asymmetry: 2. Parameterization and fitting to observations, *J. Geophys. Res.*, *107*(A8), 1176, doi:10.1029/2001JA000220.

Ungstrup, E., and I. M. Jackerott (1963), Observations of chorus below 1500 cycles per second at Godhavn, Greenland from July 1957 to December 1961, *J. Geophys. Res.*, *68*, 2141–2146.

Vaivads, A., O. Santolík, G. Stenberg, M. André, C. J. Owen, P. Canu, and M. Dunlop (2007), Source of whistler emissions at the dayside magnetopause, *Geophys. Res. Lett.*, *34*, L09106, doi:10.1029/2006GL029195.

West, H. I., Jr., R. M. Buck, and J. R. Walton (1973), Electron pitch angle distributions throughout the magnetosphere as observed on Ogo 5, *J. Geophys. Res.*, *78*, 1064–1081.

U. S. Inan and M. Spasojevic, Space, Telecommunications, and Radioscience Laboratory, Stanford University, 350 Serra Mall, Stanford, CA 94305-9515, USA. (mariaspasojevic@stanford.edu)